



Published in final edited form as:

Neuron. 2014 November 19; 84(4): 764–777. doi:10.1016/j.neuron.2014.09.030.

A TRPV Channel in *Drosophila* Motor Neurons Regulates Presynaptic Resting Ca²⁺ Levels, Synapse Growth, and Synaptic Transmission

Ching-On Wong¹, Kuchuan Chen², Yong Qi Lin^{3,4,5}, Yufang Chao¹, Lita Duraine^{3,4}, Zhongmin Lu⁶, Wan Hee Yoon^{3,4}, Jeremy M. Sullivan⁷, Geoffrey T. Broadhead¹, Charlotte J. Sumner^{7,8}, Thomas E. Lloyd^{7,8}, Gregory T. Macleod^{9,10}, Hugo J. Bellen^{2,3,4}, and Kartik Venkatachalam^{1,2,11,12}

¹Department of Integrative Biology and Pharmacology, University of Texas School of Medicine, 6431 Fannin Street, Houston, TX 77030, USA

²Graduate Program in Developmental Biology, Baylor College of Medicine, 1250 Moursund Street, Suite N1125.14, Mailstop NR-1125, Houston, TX 77030, USA

³Howard Hughes Medical Institute, 1250 Moursund Street, Suite N1125.14, Mailstop NR-1125, Houston, TX 77030, USA

⁴Departments of Molecular and Human Genetics and Neuroscience, Baylor College of Medicine, 1250 Moursund Street, Suite N1125.14, Mailstop NR-1125, Houston, TX 77030, USA

⁶Integrative Biology and Neuroscience program, Florida Atlantic University and Max Planck Florida Institute, 5353 Parkside Drive, Jupiter, FL 33458, USA

⁷Department of Neurology, Johns Hopkins University School of Medicine, 855 North Wolfe Street, Baltimore, MD 21231, USA

⁸Department of Neuroscience, Johns Hopkins University School of Medicine, 855 North Wolfe Street, Baltimore, MD 21231, USA

⁹Department of Physiology, University of Texas Health Science Center, 7703 Floyd Curl Drive, San Antonio, TX 78229, USA

¹¹Graduate Programs in Cell and Regulatory Biology (CRB) and Neuroscience, Graduate School of Biomedical Sciences, University of Texas School of Medicine, Houston, TX 77030

SUMMARY

© 2014 Elsevier Inc. All rights reserved.

¹²Correspondence: kartik.venkatachalam@uth.tmc.edu.

⁵Current address: Functional Genomics Group, Neuroscience Program, Garvan Institute of Medical Research, 384 Victoria St, Darlinghurst NSW 2010, Australia

¹⁰Current address: Department of Biological Sciences, Florida Atlantic University, 5353 Parkside Drive, Jupiter, FL 33458, USA

Publisher's Disclaimer: This is a PDF file of an unedited manuscript that has been accepted for publication. As a service to our customers we are providing this early version of the manuscript. The manuscript will undergo copyediting, typesetting, and review of the resulting proof before it is published in its final citable form. Please note that during the production process errors may be discovered which could affect the content, and all legal disclaimers that apply to the journal pertain.

The authors declare no conflicts of interest.

Presynaptic resting Ca^{2+} influences synaptic vesicle (SV) release probability. Here, we report that a TRPV channel, Inactive (*Iav*), maintains presynaptic resting $[\text{Ca}^{2+}]$ by promoting Ca^{2+} release from the endoplasmic reticulum in *Drosophila* motor neurons, and is required for both synapse development and neurotransmission. We find that *Iav* activates the Ca^{2+} /calmodulin-dependent protein phosphatase, calcineurin, which is essential for presynaptic microtubule stabilization at the neuromuscular junction. Thus, loss of *Iav* induces destabilization of presynaptic microtubules resulting in diminished synaptic growth. Interestingly, expression of human TRPV1 in *Iav*-deficient motor neurons rescues these defects. We also show that the absence of *Iav* causes lower SV release probability and diminished synaptic transmission, whereas *Iav* overexpression elevates these synaptic parameters. Together, our findings indicate that *Iav* acts as a key regulator of synaptic development and function by influencing presynaptic resting $[\text{Ca}^{2+}]$.

INTRODUCTION

At any time, the Ca^{2+} concentration ($[\text{Ca}^{2+}]$) within presynaptic terminals is a function of the complex interplay between events driving Ca^{2+} elevation and Ca^{2+} sequestration. Presynaptic Ca^{2+} elevation, which may occur due to depolarization-induced opening of voltage gated Ca^{2+} channels (VGCCs) triggers SV exocytosis (Catterall, 2000). While VGCCs are closed, the resting $[\text{Ca}^{2+}]$ is insufficient to trigger SV release, but influences SV release probability and sculpts the spatiotemporal dynamics of synaptic transmission (Awatramani et al., 2005; Zucker and Regehr, 2002). However, whether resting $[\text{Ca}^{2+}]$ is involved in other aspects of presynaptic function and whether specific non-excitatory channels set the resting $[\text{Ca}^{2+}]$ remain unknown.

We sought to evaluate the synaptic function of Ca^{2+} channels belonging to the Transient Receptor Potential (TRP) superfamily, which are voltage-independent channels that regulate diverse neuronal pathways (Venkatachalam and Montell, 2007). However, the biggest hurdle to evaluating the role of TRP channels in synapse development and function is the extent of functional redundancy between the different vertebrate TRP genes (Venkatachalam and Montell, 2007). This problem can be overcome by using *Drosophila* because flies express only 13 TRP genes compared to the 27 in vertebrates (Venkatachalam and Montell, 2007). Moreover, loss of function mutations in all 13 *Drosophila* TRP genes are available (Fowler and Montell, 2012). We found that loss of function mutations in a *Drosophila* TRPV channel gene, *inactive (iav)* (Gong et al., 2004), result in decreased synaptic growth and diminished neurotransmission. Our results indicate that *Iav* functions in motor neurons to regulate ER Ca^{2+} release and is required for maintaining presynaptic resting $[\text{Ca}^{2+}]$, which is essential for microtubule stability, synaptic growth, and SV release probability.

RESULTS

Inactive is required for synapse growth and morphology

We determined the number of synaptic boutons at the *Drosophila* 3rd instar larval NMJs in wild-type and loss-of-function alleles of the TRP channel genes indicated in Supplemental table 1 using antibodies against HRP (Horseradish peroxidase: detects a carbohydrate moiety present on numerous neuronal glycoproteins (Snow et al., 1987) and DLG (Discs

large: *Drosophila* ortholog of PSD-95 (Cho et al., 1992)). Only the larvae lacking *iav* (Gong et al., 2004) exhibit fewer synaptic boutons (muscles 6/7), which are 2-fold larger than control boutons (Supplemental table 1, Figures 1A-1B, 1G, and 1I). The *iav* mutants (*iav^l*) also exhibit diminished bouton numbers at the NMJs on muscle 4 (Figures 1D-1E and 1H). The alterations in bouton numbers and size are rescued by a genomic wild-type *iav* transgene (P[*iav⁺*]) (Figures 1C, 1F and 1G-1I). The *iav^l/Df1*, *iav^l/Df2*, *iav^{362l}*, and *iav^l/iav^{362l}* larvae (Gong et al., 2004) also show similar alterations in the bouton number and morphology (Figure 1G).

***iav* functions in motor neurons to regulate NMJ synapse growth**

To assess whether synaptic growth defects in *iav^l* are due to a requirement for Iav in motor neurons (MNs), we first expressed an RNAi against *iav* (*UAS-iav^{IR}*) in MNs using the *VGLUT^{ok371}-GAL4* (*ok371-GAL4*) driver. Expression of *iav^{IR}* in wild-type MNs induces a significant decrease in NMJ bouton number—a phenotype not observed in the *UAS/GAL4* controls (Figure 1G). Furthermore, expression of *UAS-iav* in the *iav^l* MNs using two separate drivers, *ok371-GAL4* and *d42-GAL4*, rescues the synaptic growth defects (Figure 1J).

iav is expressed in chordotonal neurons where it is required for hearing (Gong et al., 2004). However, we found that expression of *UAS-iav* in the *iav^l* chordotonal organs using *ato-Gal4* (*iav^l; ato>iav*) does not suppress the NMJ phenotype (Figure 1J). Expression of *iav* in mutant muscles (*iav^l; mef2>iav*) also does not restore the bouton number in *iav^l* (Figure 1J). These data indicate that Iav functions cell-autonomously in MNs to drive synaptic growth.

Human TRPV1, but neither human TRPV4 nor *Drosophila* Nanchung, rescue the *iav^l* synaptic growth phenotype

Within the hTRPV channel subfamily (hTRPV1-6, 25-27% identity and 39-46% similarity with Iav), hTRPV1 and hTRPV4 are the most extensively studied channels (Caterina et al., 2000; Caterina et al., 1999; Güler et al., 2002; Watanabe et al., 2002), whose activity can be manipulated by a host of pharmacological agents (Watanabe et al., 2002; Xia et al., 2011a; Xia et al., 2011b). Here, we asked whether expression of either hTRPV1 or hTRPV4 in *iav^l* MNs would suppress the synaptic growth defects (see Figure S1 for a comparison of the amino acid sequences of Iav, hTRPV1, and hTRPV4). Remarkably, expression of hTRPV1 in the *iav^l* MNs (*iav^l; ok371>hTRPV1*) suppresses the diminished synaptic growth (Figures 2A-2B, and 2J). However, expression of hTRPV1 in wild-type MNs (*ok371>hTRPV1*) does not promote the formation of additional boutons (Figures 2C and 2J). We also pharmacologically inhibited the hTRPV1 channels expressed in the *iav^l* MNs by feeding the *iav^l; ok371>hTRPV1* larvae the TRPV1 antagonist, capsazepine (CPZ) (Zygmunt et al., 1999). CPZ reverses the hTRPV1-mediated suppression of the *iav^l* synaptic growth phenotype in a dose-dependent manner (Figures 2D-2F and 2K), whereas even 300 μ M of CPZ does not decrease synaptic growth in control *iav^l*; P[*iav⁺*] neurons that lack hTRPV1 (Figure 2L). In contrast, expression of neither hTRPV4 nor *Drosophila* Nanchung (Nan—the second TRPV gene in *Drosophila* (Kim et al., 2003)) in the *iav^l* MNs suppresses the synaptic growth defects (Figure 2J).

To test whether elevating MN neuronal activity is sufficient to suppress the *iav¹* synaptic growth phenotype, we expressed a constitutively active bacterial Na⁺ channel, NaChBac (Kuzmenkin et al., 2004; Luan et al., 2006), in the *iav¹* MNs. NaChBac depolarizes the host neurons and decreases their threshold for firing action potentials (Kuzmenkin et al., 2004). In contrast to the rescue we observed with expression of hTRPV1, the *iav¹* NMJ synaptic growth defects persist following the expression of NaChBac (Figures 2G-2I, and 2M). These data indicate that the synaptic growth phenotype at the *iav¹* NMJs depends on the selective loss of TRPV channel activity rather than diminished MN excitability.

Decreased microtubule stability in *iav¹* motor neurons

The decrease in synaptic bouton number with a concomitant increase in bouton volume in *iav¹* is reminiscent of the phenotype observed in larvae lacking genes such as *wingless* (Miech et al., 2008; Packard et al., 2002), *vapb* (encoding Vesicle Associated Membrane Protein-B) (Nishimura et al., 2004; Pennetta et al., 2002), *futsch* (the fly ortholog of the gene encoding mammalian microtubule associated protein-1b (MAP-1b)) (Roos et al., 2000; Zhang et al., 2001), and *pp2A-B'* (a subunit of the PP2A protein phosphatase) (Viquez et al., 2006). Because diminished stability of presynaptic microtubules underlies the synaptic defects in these mutants, we assessed the structure of the presynaptic microtubules in *iav¹*. First, we found that the number of the characteristic Futsch loops is reduced by ~50% within *iav¹* synapses compared to controls (Figures 3A-3E). Moreover, in contrast to the Futsch loops within control boutons (Figure 3B, *arrow* points to a Futsch loop), Futsch appears punctate within some *iav¹* boutons (Figure 3D, *red arrows* point to Futsch punctae). Next, 3D reconstructions of synaptic boutons stained with an anti-Tubulin antibody revealed the characteristic loop-like structures that microtubules form within wild-type boutons (Figures 3F and *dashed lines* in 3G). However, microtubules appear fragmented in *iav¹* boutons (Figure 3H, *arrows*) further indicating that the presynaptic microtubules exhibit diminished stability at the *iav¹* NMJs.

Diminished calcineurin activity underlies the synaptic growth defects in *iav¹*

The stability of presynaptic microtubules depends on the level and/or phosphorylation status of Futsch (Franco et al., 2004; Miech et al., 2008; Packard et al., 2002; Roos et al., 2000) (Figure 3I). Thus, *futsch*-deficient larvae exhibit diminished bouton numbers and increased bouton size (Roos et al., 2000)—a phenotype similar to that observed in *iav¹*. The *Drosophila* homolog of glycogen synthase kinase-3 β (GSK-3 β), Shaggy (Sgg), phosphorylates Futsch, causing the latter to dissociate from microtubules (Franco et al., 2004; Gogel et al., 2006; Miech et al., 2008) (Figure 3I). Following the dissociation of Futsch, microtubules become destabilized and fragmented (Figure 3I) resulting in the formation of fewer boutons, which are increased in size (Franco et al., 2004; Miech et al., 2008). The protein phosphatase, calcineurin, counteracts the kinase activity of GSK-3 β by dephosphorylating microtubule-associated proteins resulting in microtubule stabilization (Figure 3I) (Gong et al., 2000a; Gong et al., 2000b). Because calcineurin is a Ca²⁺/calmodulin-activated protein phosphatase (Lynch and Michalak, 2003; Rinne et al., 2009), we hypothesized that loss of *Iav*-dependent cytosolic Ca²⁺ elevations may result in diminished calcineurin activity, which in-turn may affect microtubule stability (Figure 3I). Indeed, knocking-down *Drosophila* calcineurin (*can1*) in wild-type MNs using two RNAi

lines (*UAS-canAI^{IR}* and *UAS-canAI^{FB5}*) (Dijkers and O'Farrell, 2007) results in decreased number of synaptic boutons compared to controls (Figures 4A-4B and 4O and S2A-S2B and S2G). Furthermore, larvae that carried the *canAI* loss of function allele (Nakai et al., 2011) in *trans* with a deficiency uncovering *canAI* locus (*canAI^{-Df-canAI}*) exhibit decreased bouton numbers compared to the *canAI^{-/+}* heterozygotes (Figures S2C-S2D and S2G). However, MN specific knockdown of *canAI* in *iav¹* does not further decrease synaptic growth (Figures 4C and 4O), suggesting that *canAI* and *iav* may function in a common pathway. Loss of CanA1 also results in an increase in bouton area (Figure S2H) and destabilization of presynaptic microtubules (Figures 4D-4E, *white arrows* in Figure 4E point to fragmented tubulin within boutons). These data indicate that presynaptic loss of calcineurin decreases synaptic growth, increases the size of the boutons, and causes presynaptic microtubule destabilization at the larval NMJ—phenotypes that bear striking resemblance to those displayed by *iav¹*.

We also found that expression of a constitutively active CanA1, which does not require elevations in cytosolic Ca^{2+} to be fully active (*UAS-canAI^{CA}*) (Dijkers and O'Farrell, 2007)), in the *iav¹* MNs suppresses the synaptic growth defects (Figures 4F and 4P), whereas expression of CanA1^{CA} in wild-type MNs does not affect the overall bouton numbers (Figures 4G and 4P). Expression of CanA1^{CA} in the *iav¹* MNs also restores the bouton size (Figure S2H) and the number of Futsch loops within the NMJ boutons (Figures 4H-4K and 4Q), but does not affect the number of Futsch loops in wild-type animals (Figure 4Q). However, overexpression of CanA1^{CA} in the MNs of the *futsch* hypomorphs, *futsch^{N94}* (Roos et al., 2000), does not suppress the observed synaptic growth deficits (Figure S2I). These epistatic analyses indicate that *futsch* functions downstream of *canAI*, which in turn functions downstream of *iav*, in the regulation of synaptic growth.

Finally, if calcineurin function is decreased in *iav¹*, lowering the activity of the counteracting kinase, Sgg, may suppress the *iav¹* synaptic growth phenotype. Indeed, expression of dominant negative *sgg* (*sgg^{DN}*) in the *iav¹* MNs also suppresses the synaptic growth defects (Figures 4L-4N and 4R). Together, these findings indicate that diminished calcineurin activity underlies the synaptic growth defects observed in *iav¹*.

ER Ca^{2+} release regulates NMJ synapse morphology and development

Because calcineurin function is promoted by ER Ca^{2+} release (Lynch and Michalak, 2003; Rinne et al., 2009)), we first assessed whether ER Ca^{2+} release plays a role in NMJ synapse development. If so, depleting the MN ER Ca^{2+} stores may alter the number and size of the NMJ boutons. Indeed, RNAi-mediated knockdown of the ER Ca^{2+} pump, SERCA (*ok371* > *serca^{IR}*), which is required for maintaining Ca^{2+} levels within the ER lumen (Dormer et al., 1993; Sanyal et al., 2005)), leads to decreased synaptic growth (Figures 5A-5B and 5J). Similar results were obtained with *Kum¹⁷⁰*, a dominant-negative SERCA allele (Sanyal et al., 2005) (Figures 5D and 5J). Knockdown of SERCA in MNs also results in an increase in the size of NMJ boutons (Figure 5K)—morphological alterations reminiscent of the *iav¹* synapses.

Next, we examined the effects of lowering ER Ca^{2+} release by decreasing the levels of the genes encoding the ER Ca^{2+} release channels, ryanodine receptor and inositol trisphosphate

receptor (*RyR* and *itpr* respectively) (Hasan and Rosbash, 1992). Loss of a single copy of *RyR* (*RyR^{16/+}*), which results in diminished ER Ca^{2+} release (Sullivan et al., 2000), leads to a decrease in the number and an increase in the size of the NMJ boutons (Figures 5E and 5J-5K). Similarly, presynaptic expression of an RNAi against *itpr* (*UAS-itpr^{IR}*) using pan-neuronal or MN specific drivers (*elav>itpr^{IR}* and *ok371>itpr^{IR}* respectively) leads to reduced NMJ bouton numbers (Figure 5J). Importantly, none of these manipulations enhance the *iav¹* synaptic phenotypes (Figures 5C, 5F, and 5J; n.s., $p > 0.05$, one-way ANOVA). We also asked whether promoting ER Ca^{2+} release in *iav¹* would suppress the synaptic growth defects. To promote ER Ca^{2+} release we used the *RyR^{24D03/+}* flies that carry one extra copy of the *RyR* gene and exhibit elevated ER Ca^{2+} release (Gao et al., 2013). Remarkably, introduction of *RyR^{24D03/+}* leads to a partial suppression of the *iav¹*-associated alterations in bouton numbers (Figures 5G and 5L). These data indicate that the *iav¹* synaptic growth defects arise as a result of diminished Ca^{2+} release from the ER.

Because the MN ER traverses the axons and is found at the NMJs, defects in extension of ER into the axon terminus may also result in decreased Ca^{2+} release. Thus, we evaluated ER distribution in the *iav¹* NMJs by expressing the ER marker, Lysozyme-KDEL::GFP (using *UAS-Lyso::GFP-KDEL*; herein referred to as KDEL-GFP). Consistent with previous observations (Chouhan et al., 2010), we found that ER is distributed throughout the MN axons, and is also located within some, but not all, of the synaptic boutons (Figure 5H; *arrows* indicate ER in distal boutons). Despite an obvious decrease in the total number of boutons, presynaptic KDEL-GFP distribution is largely unchanged in *iav¹* compared to controls (Figure 5I; *arrows* indicate ER in distal boutons). Therefore, ER trafficking to the axon terminal is not significantly altered in *iav¹*.

Expression of channels that promote ER Ca^{2+} release results in a partial depletion of the ER Ca^{2+} stores in cultured cells (Wegierski et al., 2009). We evaluated whether *Iav*, TRPV1, and TRPV4 expression in Neuro2A (N2A) cells results in lower ER Ca^{2+} levels. Expression of either *Iav* or TRPV1 in N2A cells results in a ~50% decrease in ER Ca^{2+} levels (Figure 5M). However, expression of TRPV4 does not affect the ER Ca^{2+} content (Figure 5M). Together, these data are consistent with a role for *Iav* and TRPV1 in regulating ER Ca^{2+} release, which is essential for synaptic development.

***iav* and hTRPV1, but not hTRPV4, localize to the ER**

Next, we sought to identify the subcellular distribution of *Iav* and TRPV1 in larval MNs. Although we could detect *Iav* in larval chordotonal organs using established antibodies (Gong et al., 2004) (Figure S3A), we could not detect *Iav* in wild-type larval MNs using these antibodies. These findings are consistent with the difficulties in observing the native expression patterns of some Ca^{2+} channels owing to their low expression levels (Ly et al., 2008; Venkatachalam et al., 2008). Therefore, we evaluated whether *Iav* overexpression, which suppresses the *iav¹* phenotypes, would reveal the protein's subcellular distribution. We found that overexpressed *Iav* colocalized with KDEL::GFP in MN cell bodies (Figures 6A-6C) and muscle (Figure S3B). Using anti-TRPV1 antibodies (Tominaga et al., 1998), we found that hTRPV1 also colocalizes with KDEL-GFP in the MN cell bodies (Figures 6D-6F). In contrast, hTRPV4 overexpressed in MNs does not show overlap with KDEL-

GFP (Figures 6G-6I, *arrowheads* point to hTRPV4 expression). Hence, both *Iav* and hTRPV1, which suppress the NMJ defects observed in *iav¹*, are expressed in the ER, whereas hTRPV4, which does not suppress the *iav¹* NMJ growth defects, is not localized to the ER.

Loss of *Iav* results in decreases in presynaptic resting $[Ca^{2+}]$

Next, we asked whether loss of *Iav* results in diminished cytosolic $[Ca^{2+}]$ at NMJ termini. To evaluate resting $[Ca^{2+}]$ within presynaptic boutons, we expressed GCaMP5G (GCaMP) (Akerboom et al., 2012) linked via a 2A peptide (P2A) to tdTomato (tdT)—a Ca^{2+} insensitive fluorescent protein (Figure 7A) (Daniels et al., 2014). The 2A peptide is cleaved by native endoproteases in *Drosophila* neurons (Inagaki et al., 2012), leading to the separation of GCaMP5G from tdTomato—both of which are expressed at the NMJ (Figure 7B). Because the two fluorophores are translated as a single polypeptide, the levels of tdTomato can be used to normalize the levels of GCaMP5G. This ratiometric normalization is important for determining resting $[Ca^{2+}]$, which does not involve the measurement of robust alterations from baseline. Our analysis revealed that the relative ratio of the GCaMP5G:tdTomato fluorescence intensities in WT and *iav¹* are comparable when the recordings are performed in extracellular bath solution containing 1.5 mM $[Ca^{2+}]$ (Figure 7C). However, when the bath $[Ca^{2+}]$ over the same NMJs is dropped to 0.5 mM and 0 mM, the intensity ratios show a significant decline in *iav¹* boutons (Figure 7C). Remarkably, the intensity ratio at WT NMJs does not change even after 9 minutes in a solution containing no Ca^{2+} . These data indicate that the resting cytosolic $[Ca^{2+}]$ at NMJ bouton terminals is sustained by release of Ca^{2+} from intracellular stores and the ability of these stores to maintain presynaptic resting $[Ca^{2+}]$ is compromised in *iav¹*.

Loss of *Iav* results in diminished synaptic transmission and SV release probability

We hypothesized that owing to the critical roles of presynaptic Ca^{2+} in SV release and synaptic transmission (Jahn and Fasshauer, 2012), evoked excitatory junctional potentials (EJPs) may be diminished at *iav¹* NMJs. Indeed, at 0.5 mM extracellular $[Ca^{2+}]$ ($[Ca^{2+}]_{ext}$), the EJP amplitudes are ~50% lower at the *iav¹* NMJs compared to controls (Figures 7D-7E). However, *canA1* deficient NMJs, which also show a decrease in the number of synaptic boutons, do not exhibit a corresponding decrease in EJP amplitude (Figure 7E). Thus, although *Iav* regulates NMJ growth and morphology via calcineurin, *Iav* regulates synaptic transmission independent of calcineurin.

We also found that the amplitude and frequency of spontaneous mini-EJPs (mEJPs) are unchanged in *iav¹* (Figures S4A-S4B). Hence, the quantal content (EJP amplitude/mEJP amplitude), indicative of the number of SVs released per evoked event, is ~50% decreased in *iav¹* (Figure 7F). The diminished EJP and quantal content in *iav¹* are rescued by expression of *UAS-iav* in MNs (Figures 7E-7F).

If the decreased quantal content at *iav¹* NMJs is a consequence of a decrease in presynaptic resting $[Ca^{2+}]$, raising $[Ca^{2+}]_{ext}$ during neurotransmission may restore the quantal content. To test this hypothesis, we recorded quantal contents at $[Ca^{2+}]_{ext}$ concentrations of 0.25 mM, 0.4 mM, and 0.75 mM. We found that the relative decrease in quantal content in *iav¹* is

most severe at 0.25 mM $[Ca^{2+}]_{ext}$ (~70% lower than in controls), and becomes progressively less pronounced at higher $[Ca^{2+}]_{ext}$ (Figures S4C and 7G). At 0.75 mM $[Ca^{2+}]_{ext}$, the quantal content in *iav^l* is not significantly different than in controls (Figures S4C and 7G, $p = 0.6$, unpaired Student's t-test, $n = 4-5$ NMJs per genotype). These data indicate that the synaptic transmission defects in *iav^l* are primarily a consequence of diminished presynaptic resting Ca^{2+} levels, which can be suppressed by increasing the amounts of Ca^{2+} entering the boutons through the VGCC.

Examination of the presynaptic ultrastructure by electron microscopy revealed that the *iav^l* NMJs do not display significant alterations in other parameters involved in regulating SV release (Figures S5A-S5C). Previous studies have found a 3rd-4th order dependence of neurotransmitter release upon $[Ca^{2+}]_{ext}$, and this cooperativity is decreased in mutations affecting the levels of the SV Ca^{2+} sensor, Synaptotagmin (Jan and Jan, 1976; Littleton et al., 1994). The Ca^{2+} cooperativity also reflects the number of VGCCs participating in the release of a single SV (Matveev et al., 2011). We found that Ca^{2+} cooperativity of neurotransmitter release in both controls and *iav^l* larvae, as determined by the slopes of the double-logarithmic plots of quantal content and $[Ca^{2+}]_{ext}$ (Jan and Jan, 1976; Littleton et al., 1994) remains unchanged (Figure S4C, slopes in control and *iav^l* are 3.4 and 3.5 respectively). Taken with the lack of alterations in SV number or distribution in *iav^l*, these data argue against a role for an exocytic block in the *iav^l* neurotransmission defects.

Cytosolic Ca^{2+} concentration at axon terminals influences SV release probability, which can be evaluated using the paired-pulse ratio of evoked potentials (Zhang et al., 2009; Zucker and Regehr, 2002). When the resting $[Ca^{2+}]$ at a synapse is low, stimulus-induced elevation in presynaptic $[Ca^{2+}]$ will induce the exocytosis of relatively fewer synaptic vesicles resulting in a smaller evoked EJP. However, if a second stimulus, i.e. the paired-pulse, is provided before the resting Ca^{2+} returns to baseline, the presynaptic Ca^{2+} will elevate sufficiently leading to the exocytosis of the remaining SVs. Therefore, the higher the ratio of amplitudes of evoked responses following the first and second pulses respectively (known as paired pulse facilitation), the lower is the probability of SV release, and *vice versa*. Consistent with the observation that the *iav^l* NMJ synapses have reduced SV release probability, the paired-pulse ratio is increased by ~50% at *iav^l* NMJs (Figures 7H-7I). Expression of *UAS-iav* in the *iav^l* MNs restores the SV release probability (Figure 7I).

Overexpression of *iav* in wild-type MNs results in increased SV release probability and neurotransmission

If *iav* is a determinant of presynaptic resting Ca^{2+} levels, raising its expression level may sensitize the synapse to releasing more SVs. Indeed, overexpression of *iav* in wild-type MNs leads to a ~50% increase in EJP amplitude and quantal content (Figures 7J-7K). We also found that the elevation in EJP amplitudes following *iav* overexpression is a consequence of increased SV release probability as determined by a decrease in the paired-pulse ratio (Figure 7L). Interestingly, overexpression of *iav* in MNs also results in the formation of fewer synaptic boutons indicating that the number of synaptic boutons at the larval NMJ exhibits a bell-shaped dependence on the expression levels of *iav* (Figure S5H). We also found that overexpression of *RyR* or *Itpr* also leads to the formation of fewer synaptic

boutons at the *Drosophila* NMJ (data not shown). Thus, the consequence of *iav* overexpression on the number of synaptic boutons is likely due to an increase in presynaptic Ca^{2+} rather than a specific effect of *Iav* *per se*. However, overexpression of *iav* in the MNs does not lead to an increase in the total number of punctae formed by the active zone (AZ) specific structural protein, Bruchpilot (Brp) (Kittel et al., 2006) (Figure S5I, $p = 0.4$, unpaired Student's *t*-test). Therefore, SV release increases following *iav* overexpression are a consequence of elevated resting Ca^{2+} levels rather than due to alterations in the number of SV release sites.

DISCUSSION

***iav*-mediated calcineurin activation regulates presynaptic microtubule stability, bouton morphology, and bouton numbers**

Here we show that *Iav* functions in larval MNs to regulate the development and function of the NMJ. Although expression *UAS-iav* in the *iav¹* MNs rescues the defects in NMJ growth and synaptic transmission, this does not alter the *iav¹* locomotion defects (data not shown). In contrast, expression of *UAS-iav* in the *iav¹* chordotonal neurons suppresses the locomotion defects (data not shown) but does not impact the NMJ phenotypes. Thus, the *iav¹* NMJ and proprioceptive phenotypes arise separately in the MNs and chordotonal neurons respectively.

The phenotype of diminished synaptic bouton numbers with an increase in bouton size observed in *iav¹* occurs due to destabilization of presynaptic microtubules. Furthermore, our investigation revealed that in the absence of *Iav*, presynaptic microtubule stability and bouton numbers are diminished due to decreased calcineurin activity. Thus, constitutively active *calcineurin* suppresses these *iav¹* phenotypes. However, expression of the constitutively active *calcineurin* does not suppress the synaptic growth defects in the *futsch* hypomorphs, indicating that *futsch* functions downstream of *calcineurin*. Previous studies have also implicated the other Ser/Thr protein phosphatase, PP2A, in regulating microtubule stability and NMJ development by antagonizing Sgg (Viquez et al., 2009; Viquez et al., 2006). Because PP2A is Ca^{2+} -independent, these observations suggest that distinct signals can lead to similar alterations in NMJ synapse morphology via *Futsch*.

The transcription factor, nuclear factor of activated T-cells (NFAT) is activated by calcineurin (Clipstone and Crabtree, 1992; Jain et al., 1993). However, our findings suggest the *iav¹* and *calcineurin* mutant phenotypes studied here are unlikely to be NFAT dependent because NFAT knockouts display an increase in bouton number (Freeman et al., 2011) rather than the decrease observed in the *iav¹* and *calcineurin* mutants. Thus, in the context of NMJ synapse development, calcineurin appears to function via *Futsch* rather than NFAT.

***iav* regulates ER Ca^{2+} release and presynaptic resting $[\text{Ca}^{2+}]$ in *Drosophila* larval MNs**

Several lines of evidence indicate that *Iav* and TRPV1 regulate ER Ca^{2+} release. First, decreasing ER Ca^{2+} release independent of *Iav* recapitulates the *iav¹* synaptic growth and morphological phenotypes. Moreover, loss of SERCA results in decreased EJP amplitude but normal mini frequency and amplitudes (Sanyal et al., 2005)—defects similar to those

observed in *iav*¹. Second, elevated ER Ca²⁺ release via RyR suppresses the *iav*¹ synaptic growth and morphological phenotypes. Third, expression of *Iav* or TRPV1 in N2A cells results in the partial depletion of ER stores. Fourth, overexpressed *Iav* and TRPV1 are localized to the ER in the MN cell bodies. Interestingly, native TRPV1 in mammalian DRG neurons have been shown to localize to the ER and also permit ER Ca²⁺ release (Castro et al., 2009; Gallego-Sandin et al., 2009), although the biological significance of TRPV1 in the ER has so far remained unknown. The ER localization of *Iav* and TRPV1 is not simply an artifact of overexpression of a membrane protein because overexpressed hTRPV4 is not localized to the ER in MN cell bodies. Most importantly, *Iav* is required for maintaining synaptic resting [Ca²⁺] in the absence of extracellular Ca²⁺. These data strongly support the notion that *Iav* regulates Ca²⁺ release from an intracellular store to maintain the presynaptic resting [Ca²⁺]. Several studies have found that the ionic environment in the synaptic cleft could be tightly insulated such that [Ca²⁺] in synaptic clefts can drop dramatically during bursts of synaptic transmission thereby severely limiting Ca²⁺ entry into the presynaptic termini (Borst and Sakmann, 1999; Egelman and Montague, 1999; Rabl and Thoreson, 2002; Rusakov and Fine, 2003; Stanley, 2000). Although the synaptic cleft in a *Drosophila* NMJ is likely permeable to extracellular ions because these synapses are not tightly insulated by glial cells (Fuentes-Medel et al., 2009), more tightly insulated synapses such as those in vertebrate CNS might be more dependent on ER Ca²⁺ release to maintain the strength of synaptic transmission during intense stimulation.

The role of *Iav* in maintaining presynaptic resting [Ca²⁺] is not uncovered till the extracellular [Ca²⁺] is dropped to 0.5 mM. We speculate that endogenous decreases in synaptic [Ca²⁺] to the lower end of the 0.5-1.5 mM range in *iav*¹ might result in subthreshold activation of calcineurin. However, since the extracellular [Ca²⁺] at a *Drosophila larval* NMJ is not known, we cannot rule out the possibility that *Iav* regulates the activity of calcineurin via a mechanism independent of the resting [Ca²⁺].

Our findings also allow us to speculate that *Iav* could function in homeostatic control of presynaptic [Ca²⁺]. The activity of *Iav* may be suppressed at resting [Ca²⁺] via proteins such as calmodulin such that a drop in resting [Ca²⁺] could result in *Iav* disinhibition and channel opening. Indeed, ER Ca²⁺ release via TRPV1 has been shown to be strongly suppressed by calmodulin binding to a C-terminal calmodulin binding domain on TRPV1 (Gallego-Sandin et al., 2009). Interestingly, *Iav* also contains a C-terminal calmodulin binding domain, which may underlie the homeostatic control of *Iav* activity.

Evoked neurotransmission at the *Drosophila* larval NMJ depends on *Iav* dosage and presynaptic [Ca²⁺] rather than the number of release sites

Owing to its function in the regulation of presynaptic resting [Ca²⁺], *Iav* influences SV release probability and the amplitude of evoked neurotransmission without affecting the Ca²⁺ cooperativity of SV release. Furthermore, *Iav* regulates neurotransmission in a dose dependent manner consistent with a critical function of the protein in evoked neurotransmission. Although calcineurin inhibits SV cycling at the *Drosophila* NMJ (Kuromi et al., 1997) and promotes synaptic growth, calcineurin does not play a role in *Iav*-dependent regulation of synaptic transmission. Moreover, our findings indicate that

presynaptic Ca^{2+} , rather than the number of SV release sites, is the major factor in regulating the evoked SV release. Thus, at higher extracellular $[\text{Ca}^{2+}]$, the Ca^{2+} entering via the VGCC compensates for the lower resting $[\text{Ca}^{2+}]$ in *iav¹*, thereby resulting in normal synaptic transmission despite the reduction in the number of NMJ boutons and active zones (number of Brp punctae per NMJ, *iav¹;P[iav⁺]* = 413.1, *iav¹* = 339.4, $p = 0.01$, Student's *t*-test, $n = 11$ NMJs per genotype). Thus, synaptic transmission does not change proportionally with the number of synaptic boutons or even the number of active zones per synapse. Indeed, only ~50% of active zones at a *Drosophila* larval NMJ participate in SV release (Peled and Isacoff, 2011) and although both *vapb* and *futsch* mutants have fewer synaptic boutons, they exhibit elevated evoked synaptic transmission (Chai et al., 2008; Zhang et al., 2001).

EXPERIMENTAL PROCEDURES

Immunohistochemistry and confocal imaging

Wandering 3rd instar larvae were filleted in ice-cold PBS by cutting the body wall open along the dorsal midline and removing the visceral organs except the brain and nerves. The fillet was fixed in 4% PFA in PBS for 30 minutes. The fixed fillets were washed with 0.1% Triton X-100 in PBS before incubation with primary antibodies overnight at 4°C. Antibody dilutions: 1:200 rabbit anti-HRP (Jackson ImmunoResearch), 1:100 mouse anti-DLG (Parnas et al., 2001), 1:50 mouse anti-NC82 (Wagh et al., 2006), 1:50 mouse anti-Futsch (Fujita et al., 1982), 1:100 mouse anti-alpha-tubulin (Thazhath et al., 2002), 1:200 mouse anti-GFP (Invitrogen), 1:200 rabbit anti-TRPV1 and anti-TRPV4 (Alomone Labs), and 1:200 GFP-Booster (Chromotek). The rat anti-Iav antibody (anti-serum GNIEb (Gong et al., 2004)) was precleared by incubating the antibody with fixed *iav¹* fillets at a concentration of 1:100. Subsequently, the precleared antibody was used at dilution of 1:5. The monoclonal antibodies against DLG, NC82, Futsch, and alpha-tubulin were obtained from the Developmental Studies Hybridoma Bank developed under the auspices of the NICHD and maintained by The University of Iowa, Department of Biology, Iowa City, IA 52242. The samples were then washed and probed with fluorophore-conjugated secondary antibodies (1:400, Alexa Fluor 488/568/647) (Invitrogen) at room temperature for 1.5 hours and then mounted on glass slides with Vectashield (Vector Labs). Confocal images were obtained using a Nikon A1 Confocal Laser Microscope System (Nikon). For NMJ bouton counting, a 60× oil objective was used to focus on the NMJs on abdominal segment 3.

Evaluation of NMJ presynaptic $[\text{Ca}^{2+}]$ using tdTomato-P2A-GCaMP5G

3rd instar larval fillets were prepared in ice-cold HL-3.1, which contained (in mM): 70 NaCl, 5 KCl, 1.5 CaCl_2 , 4 MgCl_2 , 10 NaHCO_3 , 5 trehalose, 115 sucrose, and 5 HEPES. 7 mM L-glutamic acid was added to HL-3.1 to desensitize glutamate receptors and prevent muscle contraction during the course of experiment. The VNCs were severed from the dorsal brain lobes to prevent peristalsis. Dissected fillets were allowed to equilibrate to room temperature in HL3.1 containing 1.5 mM Ca^{2+} for at least 15 minutes before imaging. Type 1b boutons on muscle M13 of abdominal segment A4 were brought to focus with a 100× water-immersion objective on an Olympus BX51WI microscope. Images were captured with an Andor Technology EMCCD camera (DU860) under the control of Ando IQ software.

Subsequently, fluorescence signals were captured for tdTomato and for GCaMP5G. The bath solution was then exchanged to HL3.1 containing 0.5 mM CaCl₂. Two minutes after bath exchange, fluorescence signals were captured at the same settings. Bath solution was then further exchanged to nominally Ca²⁺ free HL3.1. Fluorescence signals were then captured again 2 minutes and 9 minutes after bath exchange. Recorded images were analyzed using Andor IQ software. Regions not containing an axon terminal and close to a region of interest (ROI) were selected as background. Average pixel intensity from the background regions was subtracted from that of ROI for each fluorescence channel.

Ca²⁺ imaging in N2A cells

N2A cells were cultured in DMEM (Invitrogen) supplemented with 5% fetal bovine serum. Cells were transfected with *TRPV* cDNA or control vector using X-tremeGENE 9 DNA transfection reagent (Roche) at 1:4 DNA-to-reagent ratio according to the manufacturer's instructions. One day later, transfected cells were trypsinized and seeded onto poly-D-lysine coated glass coverslips. Another day later, cells were loaded with 10 μM fura2-AM (Invitrogen) in culture medium for 30 minutes. The glass coverslips were mounted onto a chamber containing 500 μL of bath solution (125 mM NaCl, 5 mM KCl, 10 mM MgSO₄, 10 mM KH₂PO₄, 1 mM CaCl₂, 5.5 mM glucose, and 5 mM HEPES; pH 7.4). Fura-2 signals, which represent cytosolic free [Ca²⁺] were recorded by 340/380 nm excitation and 510 nm emission, using a Nikon TiE Wide-Field Fluorescence Imaging System (Nikon). The background subtracted emission ratio (R_{340/380}) was measured and calculated by NIS Elements imaging software (Nikon).

To evaluate the total ER Ca²⁺ content, we completely released the ER Ca²⁺ stores using thapsigargin (TG) while simultaneously evaluating the resulting elevation in cytosolic Ca²⁺, which is indicative of the total ER Ca²⁺ levels (Wegierski et al., 2009). Baseline fura-2 fluorescence was first acquired for 1 minute, before replacing the bath solution with Ca²⁺-free bath solution. Three minutes after removing bath Ca²⁺, 5 μM thapsigargin was added to the bath, and the fluorescence images were recorded for another 6 minutes. The amplitude of the R_{340/380} was taken to be the total ER Ca²⁺ content of those cells.

Supplementary Material

Refer to Web version on PubMed Central for supplementary material.

Acknowledgments

We thank the Bloomington *Drosophila* Stock Center for fly stocks, Dr. C. Montell for the *trpg^{G4}* and *UAS-nan* flies, Dr. T. Aigaki for the *canA1* deficient flies, Dr. S. Sanyal for the *kum¹⁷⁰* flies, Dr. P. O'Farrell for the *UAS-canA1^{FB5}* and *UAS-canA1^{CA}* lines, Drs. D. Sandstrom and B. White for the *RyR^{24D03}* flies, Dr. C. Kim for the anti-Iav antibodies, and Dr. R. Daniels for the *UAS-tdTomato-P2A-GCaMP5G* flies. We also thank Dr. C-K Yao and H. Hu for technical help. We are grateful to N. Haelterman, Dr. N. Giagtzoglou, Dr. S. Yamamoto, Dr. H. Sandoval, and Dr. M. Jaiswal for helpful discussions. H.J.B. is an Investigator of the HHMI. This work was supported by the NINDS grant, R01NS081301 (K.V.).

REFERENCES

- Akerboom J, Chen TW, Wardill TJ, Tian L, Marvin JS, Mutlu S, Calderon NC, Esposti F, Borghuis BG, Sun XR, et al. Optimization of a GCaMP calcium indicator for neural activity imaging. *J Neurosci*. 2012; 32:13819–13840. [PubMed: 23035093]
- Awatramani GB, Price GD, Trussell LO. Modulation of transmitter release by presynaptic resting potential and background calcium levels. *Neuron*. 2005; 48:109–121. [PubMed: 16202712]
- Borst JG, Sakmann B. Depletion of calcium in the synaptic cleft of a calyx-type synapse in the rat brainstem. *J Physiol*. 1999; 521(Pt 1):123–133. [PubMed: 10562339]
- Castro J, Aromataris EC, Rychkov GY, Barritt GJ. A small component of the endoplasmic reticulum is required for store-operated Ca²⁺ channel activation in liver cells: evidence from studies using TRPV1 and taurodeoxycholic acid. *Biochem J*. 2009; 418:553–566. [PubMed: 19007332]
- Caterina MJ, Leffler A, Malmberg AB, Martin WJ, Trafton J, Petersen-Zeitl KR, Koltzenburg M, Basbaum AI, Julius D. Impaired nociception and pain sensation in mice lacking the capsaicin receptor. *Science*. 2000; 288:306–313. [PubMed: 10764638]
- Caterina MJ, Rosen TA, Tominaga M, Brake AJ, Julius D. A capsaicin-receptor homologue with a high threshold for noxious heat. *Nature*. 1999; 398:436–441. [PubMed: 10201375]
- Catterall WA. Structure and regulation of voltage-gated Ca²⁺ channels. *Annu Rev Cell Dev Biol*. 2000; 16:521–555. [PubMed: 11031246]
- Chai A, Withers J, Koh YH, Parry K, Bao H, Zhang B, Budnik V, Pennetta G. hVAPB, the causative gene of a heterogeneous group of motor neuron diseases in humans, is functionally interchangeable with its *Drosophila* homologue DVAP-33A at the neuromuscular junction. *Hum Mol Genet*. 2008; 17:266–280. [PubMed: 17947296]
- Cho KO, Hunt CA, Kennedy MB. The rat brain postsynaptic density fraction contains a homolog of the *Drosophila* discs-large tumor suppressor protein. *Neuron*. 1992; 9:929–942. [PubMed: 1419001]
- Chouhan AK, Zhang J, Zinsmaier KE, Macleod GT. Presynaptic mitochondria in functionally different motor neurons exhibit similar affinities for Ca²⁺ but exert little influence as Ca²⁺ buffers at nerve firing rates in situ. *J Neurosci*. 2010; 30:1869–1881. [PubMed: 20130196]
- Clipstone NA, Crabtree GR. Identification of calcineurin as a key signalling enzyme in T-lymphocyte activation. *Nature*. 1992; 357:695–697. [PubMed: 1377362]
- Daniels RW, Rossano AJ, Macleod GT, Ganetzky B. Expression of multiple transgenes from a single construct using viral 2A peptides in *Drosophila*. *PLoS One*. 2014; 9:e100637. [PubMed: 24945148]
- Dijkers PF, O'Farrell PH. *Drosophila* calcineurin promotes induction of innate immune responses. *Curr Biol*. 2007; 17:2087–2093. [PubMed: 18060786]
- Dorner RL, Capurro DE, Morris R, Webb R. Demonstration of two isoforms of the SERCA-2b type Ca²⁺,Mg(2+)-ATPase in pancreatic endoplasmic reticulum. *Biochim Biophys Acta*. 1993; 1152:225–230. [PubMed: 8218323]
- Egelman DM, Montague PR. Calcium dynamics in the extracellular space of mammalian neural tissue. *Biophys J*. 1999; 76:1856–1867. [PubMed: 10096884]
- Fowler MA, Montell C. *Drosophila* TRP channels and animal behavior. *Life Sci*. 2012
- Franco B, Bogdanik L, Bobiniec Y, Debec A, Bockaert J, Parmentier ML, Grau Y. Shaggy, the homolog of glycogen synthase kinase 3, controls neuromuscular junction growth in *Drosophila*. *J Neurosci*. 2004; 24:6573–6577. [PubMed: 15269269]
- Freeman A, Franciscovich A, Bowers M, Sandstrom DJ, Sanyal S. NFAT regulates pre-synaptic development and activity-dependent plasticity in *Drosophila*. *Mol Cell Neurosci*. 2011; 46:535–547. [PubMed: 21185939]
- Fuentes-Medel Y, Logan MA, Ashley J, Ataman B, Budnik V, Freeman MR. Glia and muscle sculpt neuromuscular arbors by engulfing destabilized synaptic boutons and shed presynaptic debris. *PLoS Biol*. 2009; 7:e1000184. [PubMed: 19707574]
- Fujita SC, Zipursky SL, Benzer S, Ferrus A, Shotwell SL. Monoclonal antibodies against the *Drosophila* nervous system. *Proc Natl Acad Sci U S A*. 1982; 79:7929–7933. [PubMed: 6818557]

- Gallego-Sandin S, Rodriguez-Garcia A, Alonso MT, Garcia-Sancho J. The endoplasmic reticulum of dorsal root ganglion neurons contains functional TRPV1 channels. *J Biol Chem*. 2009; 284:32591–32601. [PubMed: 19778904]
- Gao S, Sandstrom DJ, Smith HE, High B, Marsh JW, Nash HA. Drosophila ryanodine receptors mediate general anesthesia by halothane. *Anesthesiology*. 2013; 118:587–601. [PubMed: 23254148]
- Gogel S, Wakefield S, Tear G, Klambt C, Gordon-Weeks PR. The Drosophila microtubule associated protein Futsch is phosphorylated by Shaggy/Zeste-white 3 at an homologous GSK3beta phosphorylation site in MAP1B. *Mol Cell Neurosci*. 2006; 33:188–199. [PubMed: 16949836]
- Gong CX, Lidsky T, Wegiel J, Zuck L, Grundke-Iqbal I, Iqbal K. Phosphorylation of microtubule-associated protein tau is regulated by protein phosphatase 2A in mammalian brain. Implications for neurofibrillary degeneration in Alzheimer's disease. *J Biol Chem*. 2000a; 275:5535–5544. [PubMed: 10681533]
- Gong CX, Wegiel J, Lidsky T, Zuck L, Avila J, Wisniewski HM, Grundke-Iqbal I, Iqbal K. Regulation of phosphorylation of neuronal microtubule-associated proteins MAP1b and MAP2 by protein phosphatase-2A and -2B in rat brain. *Brain Res*. 2000b; 853:299–309. [PubMed: 10640627]
- Gong Z, Son W, Chung YD, Kim J, Shin DW, McClung CA, Lee Y, Lee HW, Chang DJ, Kaang BK, et al. Two interdependent TRPV channel subunits, inactive and Nanchung, mediate hearing in *Drosophila*. *J Neurosci*. 2004; 24:9059–9066. [PubMed: 15483124]
- Güler AD, Lee H, Iida T, Shimizu I, Tominaga M, Caterina M. Heat-evoked activation of the ion channel, TRPV4. *J Neurosci*. 2002; 22:6408–6414. [PubMed: 12151520]
- Hasan G, Rosbash M. Drosophila homologs of two mammalian intracellular Ca(2+)-release channels: identification and expression patterns of the inositol 1,4,5-triphosphate and the ryanodine receptor genes. *Development*. 1992; 116:967–975. [PubMed: 1338312]
- Inagaki HK, Ben-Tabou de-Leon S, Wong AM, Jagadish S, Ishimoto H, Barnea G, Kitamoto T, Axel R, Anderson DJ. Visualizing neuromodulation in vivo: TANGO-mapping of dopamine signaling reveals appetite control of sugar sensing. *Cell*. 2012; 148:583–595. [PubMed: 22304923]
- Jahn R, Fasshauer D. Molecular machines governing exocytosis of synaptic vesicles. *Nature*. 2012; 490:201–207. [PubMed: 23060190]
- Jain J, McCaffrey PG, Miner Z, Kerppola TK, Lambert JN, Verdine GL, Curran T, Rao A. The T-cell transcription factor NFATp is a substrate for calcineurin and interacts with Fos and Jun. *Nature*. 1993; 365:352–355. [PubMed: 8397339]
- Jan LY, Jan YN. Properties of the larval neuromuscular junction in *Drosophila melanogaster*. *J Physiol*. 1976; 262:189–214. [PubMed: 11339]
- Kim J, Chung YD, Park DY, Choi S, Shin DW, Soh H, Lee HW, Son W, Yim J, Park CS, et al. A TRPV family ion channel required for hearing in *Drosophila*. *Nature*. 2003; 424:81–84. [PubMed: 12819662]
- Kuromi H, Yoshihara M, Kidokoro Y. An inhibitory role of calcineurin in endocytosis of synaptic vesicles at nerve terminals of *Drosophila* larvae. *Neurosci Res*. 1997; 27:101–113. [PubMed: 9100252]
- Kuzmenkin A, Bezanilla F, Correa AM. Gating of the bacterial sodium channel, NaChBac: voltage-dependent charge movement and gating currents. *J Gen Physiol*. 2004; 124:349–356. [PubMed: 15365092]
- Littleton JT, Stern M, Perin M, Bellen HJ. Calcium dependence of neurotransmitter release and rate of spontaneous vesicle fusions are altered in *Drosophila* synaptotagmin mutants. *Proc Natl Acad Sci U S A*. 1994; 91:10888–10892. [PubMed: 7971978]
- Luan H, Lemon WC, Peabody NC, Pohl JB, Zelensky PK, Wang D, Nitabach MN, Holmes TC, White BH. Functional dissection of a neuronal network required for cuticle tanning and wing expansion in *Drosophila*. *J Neurosci*. 2006; 26:573–584. [PubMed: 16407556]
- Ly CV, Yao CK, Verstreken P, Ohyama T, Bellen HJ. straightjacket is required for the synaptic stabilization of cacophony, a voltage-gated calcium channel alpha1 subunit. *J Cell Biol*. 2008; 181:157–170. [PubMed: 18391075]
- Lynch J, Michalak M. Calreticulin is an upstream regulator of calcineurin. *Biochem Biophys Res Commun*. 2003; 311:1173–1179. [PubMed: 14623303]

- Matveev V, Bertram R, Sherman A. Calcium cooperativity of exocytosis as a measure of Ca(2)+ channel domain overlap. *Brain Res.* 2011; 1398:126–138. [PubMed: 21621748]
- Miech C, Pauer HU, He X, Schwarz TL. Presynaptic local signaling by a canonical wingless pathway regulates development of the *Drosophila* neuromuscular junction. *J Neurosci.* 2008; 28:10875–10884. [PubMed: 18945895]
- Nakai Y, Horiuchi J, Tsuda M, Takeo S, Akahori S, Matsuo T, Kume K, Aigaki T. Calcineurin and its regulator sra/DSCR1 are essential for sleep in *Drosophila*. *J Neurosci.* 2011; 31:12759–12766. [PubMed: 21900555]
- Nishimura AL, Mitne-Neto M, Silva HC, Richieri-Costa A, Middleton S, Cascio D, Kok F, Oliveira JR, Gillingwater T, Webb J, et al. A mutation in the vesicle-trafficking protein VAPB causes late-onset spinal muscular atrophy and amyotrophic lateral sclerosis. *Am J Hum Genet.* 2004; 75:822–831. [PubMed: 15372378]
- Packard M, Koo ES, Gorczyca M, Sharpe J, Cumberledge S, Budnik V. The *Drosophila* Wnt, wingless, provides an essential signal for pre- and postsynaptic differentiation. *Cell.* 2002; 111:319–330. [PubMed: 12419243]
- Parnas D, Haghighi AP, Fetter RD, Kim SW, Goodman CS. Regulation of postsynaptic structure and protein localization by the Rho-type guanine nucleotide exchange factor dPix. *Neuron.* 2001; 32:415–424. [PubMed: 11709153]
- Peled ES, Isacoff EY. Optical quantal analysis of synaptic transmission in wild-type and rab3-mutant *Drosophila* motor axons. *Nat Neurosci.* 2011; 14:519–526. [PubMed: 21378971]
- Pennetta G, Hiesinger PR, Fabian-Fine R, Meinertzhagen IA, Bellen HJ. *Drosophila* VAP-33A directs bouton formation at neuromuscular junctions in a dosage-dependent manner. *Neuron.* 2002; 35:291–306. [PubMed: 12160747]
- Rabl K, Thoreson WB. Calcium-dependent inactivation and depletion of synaptic cleft calcium ions combine to regulate rod calcium currents under physiological conditions. *Eur J Neurosci.* 2002; 16:2070–2077. [PubMed: 12473074]
- Rinne A, Banach K, Blatter LA. Regulation of nuclear factor of activated T cells (NFAT) in vascular endothelial cells. *J Mol Cell Cardiol.* 2009; 47:400–410. [PubMed: 19540841]
- Roos J, Hummel T, Ng N, Klambt C, Davis GW. *Drosophila* Futsch regulates synaptic microtubule organization and is necessary for synaptic growth. *Neuron.* 2000; 26:371–382. [PubMed: 10839356]
- Rusakov DA, Fine A. Extracellular Ca²⁺ depletion contributes to fast activity-dependent modulation of synaptic transmission in the brain. *Neuron.* 2003; 37:287–297. [PubMed: 12546823]
- Sanyal S, Consoulas C, Kuromi H, Basole A, Mukai L, Kidokoro Y, Krishnan KS, Ramaswami M. Analysis of conditional paralytic mutants in *Drosophila* sarco-endoplasmic reticulum calcium ATPase reveals novel mechanisms for regulating membrane excitability. *Genetics.* 2005; 169:737–750. [PubMed: 15520268]
- Snow PM, Patel NH, Harrelson AL, Goodman CS. Neural-specific carbohydrate moiety shared by many surface glycoproteins in *Drosophila* and grasshopper embryos. *J Neurosci.* 1987; 7:4137–4144. [PubMed: 3320283]
- Stanley EF. Presynaptic calcium channels and the depletion of synaptic cleft calcium ions. *J Neurophysiol.* 2000; 83:477–482. [PubMed: 10634889]
- Sullivan KM, Scott K, Zuker CS, Rubin GM. The ryanodine receptor is essential for larval development in *Drosophila melanogaster*. *Proc Natl Acad Sci U S A.* 2000; 97:5942–5947. [PubMed: 10811919]
- Thazhath R, Liu C, Gaertig J. Polyglycylation domain of beta-tubulin maintains axonemal architecture and affects cytokinesis in *Tetrahymena*. *Nat Cell Biol.* 2002; 4:256–259. [PubMed: 11862218]
- Tominaga M, Caterina MJ, Malmberg AB, Rosen TA, Gilbert H, Skinner K, Raumann BE, Basbaum AI, Julius D. The cloned capsaicin receptor integrates multiple pain-producing stimuli. *Neuron.* 1998; 21:531–543. [PubMed: 9768840]
- Venkatachalam K, Long AA, Elsaesser R, Nikolaeva D, Broadie K, Montell C. Motor deficit in a *Drosophila* model of mucopolipidosis type IV due to defective clearance of apoptotic cells. *Cell.* 2008; 135:838–851. [PubMed: 19041749]

- Venkatachalam K, Montell C. TRP channels. *Annu Rev Biochem.* 2007; 76:387–417. [PubMed: 17579562]
- Viquez NM, Fuger P, Valakh V, Daniels RW, Rasse TM, DiAntonio A. PP2A and GSK-3 β antagonistically to regulate active zone development. *J Neurosci.* 2009; 29:11484–11494. [PubMed: 19759297]
- Viquez NM, Li CR, Wairkar YP, DiAntonio A. The B' protein phosphatase 2A regulatory subunit well-rounded regulates synaptic growth and cytoskeletal stability at the *Drosophila* neuromuscular junction. *J Neurosci.* 2006; 26:9293–9303. [PubMed: 16957085]
- Wagh DA, Rasse TM, Asan E, Hofbauer A, Schwenkert I, Durrbeck H, Buchner S, Dabauvalle MC, Schmidt M, Qin G, et al. Bruchpilot, a protein with homology to ELKS/CAST, is required for structural integrity and function of synaptic active zones in *Drosophila*. *Neuron.* 2006; 49:833–844. [PubMed: 16543132]
- Watanabe H, Davis JB, Smart D, Jerman JC, Smith GD, Hayes P, Vriens J, Cairns W, Wissenbach U, Prenen J, et al. Activation of TRPV4 channels (hVRL-2/mTRP12) by phorbol derivatives. *J Biol Chem.* 2002; 277:13569–13577. [PubMed: 11827975]
- Wegierski T, Steffl D, Kopp C, Tauber R, Buchholz B, Nitschke R, Kuehn EW, Walz G, Kottgen M. TRPP2 channels regulate apoptosis through the Ca²⁺ concentration in the endoplasmic reticulum. *EMBO J.* 2009; 28:490–499. [PubMed: 19153608]
- Xia R, Dekermendjian K, Lullau E, Dekker N. TRPV1: a therapy target that attracts the pharmaceutical interests. *Adv Exp Med Biol.* 2011a; 704:637–665. [PubMed: 21290320]
- Xia R, Samad TA, Btsh J, Jiang LH, Kays I, Stjernborg L, Dekker N. TRPV1 signaling: mechanistic understanding and therapeutic potential. *Curr Top Med Chem.* 2011b; 11:2180–2191. [PubMed: 21671876]
- Zhang C, Wu B, Beglopoulos V, Wines-Samuelson M, Zhang D, Dragatsis I, Sudhof TC, Shen J. Presenilins are essential for regulating neurotransmitter release. *Nature.* 2009; 460:632–636. [PubMed: 19641596]
- Zhang YQ, Bailey AM, Matthies HJ, Renden RB, Smith MA, Speese SD, Rubin GM, Broadie K. *Drosophila* fragile X-related gene regulates the MAP1B homolog Futsch to control synaptic structure and function. *Cell.* 2001; 107:591–603. [PubMed: 11733059]
- Zucker RS, Regehr WG. Short-term synaptic plasticity. *Annu Rev Physiol.* 2002; 64:355–405. [PubMed: 11826273]
- Zygmunt PM, Petersson J, Andersson DA, Chuang H, Sorgard M, Di Marzo V, Julius D, Hogestatt ED. Vanilloid receptors on sensory nerves mediate the vasodilator action of anandamide. *Nature.* 1999; 400:452–457. [PubMed: 10440374]

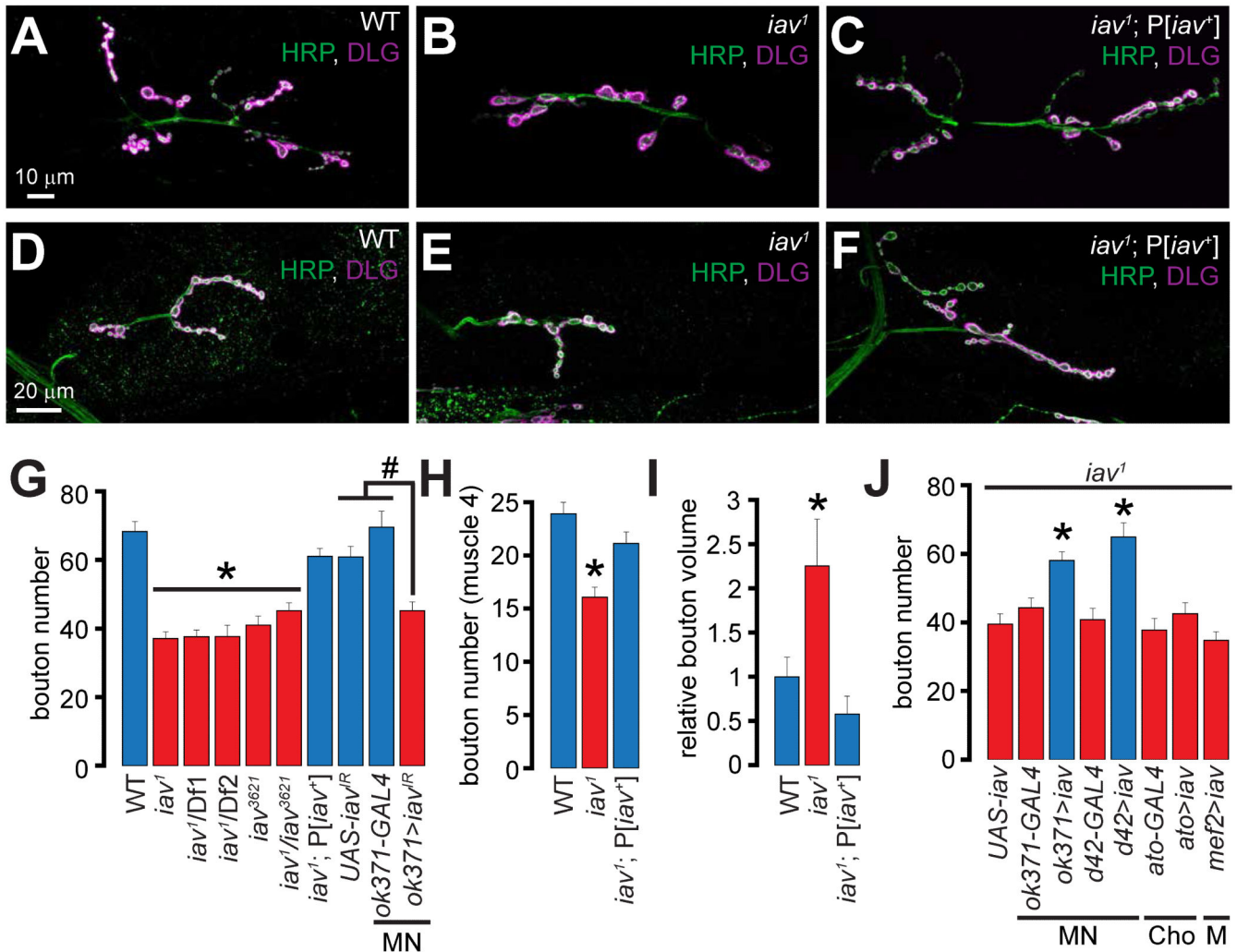


Figure 1. Alterations in synaptic growth and morphology in *iav¹*

(A-C) Confocal images of NMJs on muscles 6/7 from larvae of the indicated genotypes stained with antibodies against the presynaptic marker, HRP (green) and the postsynaptic marker, DLG (magenta). Scale bar shown in (A) also applies to (B-C).

(D-F) Confocal images of NMJs on muscle 4 from larvae of the indicated genotypes stained with antibodies against HRP (green) and DLG (magenta). Scale bar shown in (D) also applies to (E-F).

(G) Quantification of the number of boutons at NMJs on muscles 6/7 in larvae of the indicated genotypes. *, $p < 0.0001$, one-way ANOVA (comparing all the *iav¹* alleles with WT and *iav¹; P[iav⁺]*); #, $p = 2.5 \times 10^{-5}$, one-way ANOVA (comparing *ok371>iav^{IR}* with *GAL4* and *UAS* controls); $n = 8-30$ NMJs per genotype.

(H) Quantification of the number of boutons at NMJs on muscle 4 in larvae of the indicated genotypes. *, $p = 6.3 \times 10^{-6}$, one-way ANOVA (comparing all the data sets shown), $n = 8-14$ NMJs per genotype.

(I) Quantification of the volume/bouton in larvae of the indicated genotypes. *, $p = 0.007$, one-way ANOVA (comparing all the data sets shown), $n = 7$ NMJs per genotype.

(J) Quantification of the bouton number in larvae of the indicated genotypes. *, $p < 10^{-6}$, one-way ANOVA (comparing the data sets shown in the blue bars with those in the red bars), $n=11-20$ NMJs per genotype.

All values represent mean \pm SEM. Please consult Supplementary Files for values.

Abbreviations: MN, motor neuron; Cho, chordotonal organ; M, muscle.

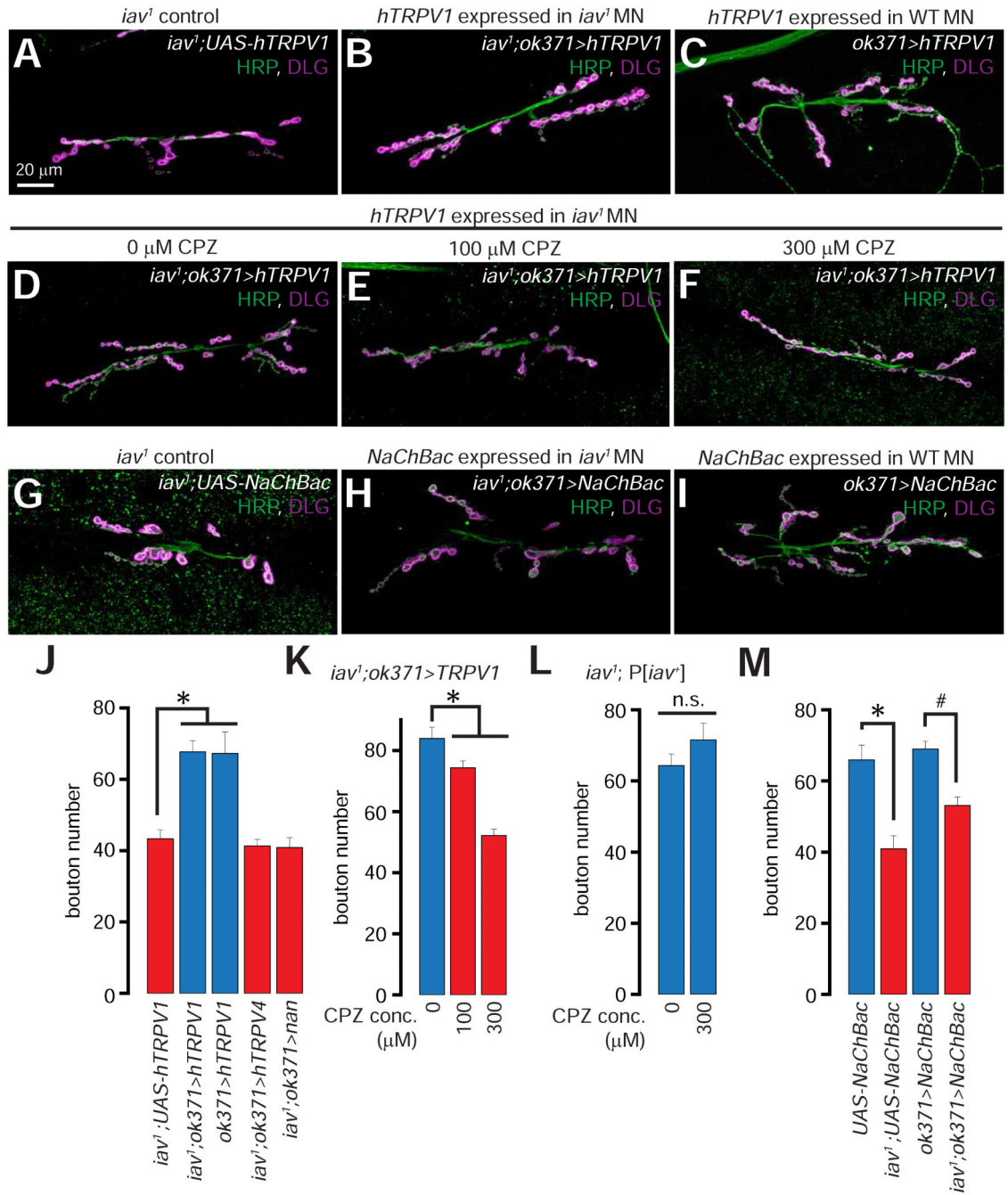


Figure 2. Suppression of *iav¹* synaptic growth defects by presynaptic expression of human TRPV1, but not human TRPV4

(A-C) Confocal images of larval NMJs from larvae of the indicated genotypes stained with antibodies against HRP (green) and DLG (magenta).

(D-F) Confocal images of larval NMJs from larvae of the indicated genotypes that were fed the indicated concentrations of capsaizene (CPZ) stained with antibodies against HRP (green) and DLG (magenta).

(G-I) Confocal images of NMJs from larvae of the indicated genotypes stained with antibodies against HRP (green) and DLG (magenta).

Scale bar shown in (A) also applies to (B-I).

(J) Quantification of the NMJ bouton number in larvae of the indicated genotypes. *, $p = 5.2 \times 10^{-4}$, one-way ANOVA, $n = 9-12$ NMJs per genotype.

(K-L) Quantification of the NMJ bouton numbers in larvae of the indicated genotypes that were fed the indicated concentrations of CPZ. The overall increased baseline of the bouton number in all the genotypes here was a result of raising the flies on instant food. In (K), *, $p = 10^{-9}$, one-way ANOVA, $n = 14-28$ NMJs per genotype. In (L), n.s. represents “not significant”, $p = 0.22$, unpaired Student’s t-test, $n = 15$ NMJs per genotype.

(M) Quantification of the NMJ bouton number in larvae of the indicated genotypes. *, $p = 4.4 \times 10^{-4}$, unpaired Student’s t-test, $n = 8-9$ NMJs per genotype; #, $p = 1.3 \times 10^{-5}$, unpaired Student’s t-test, $n = 18-24$ NMJs per genotype.

All values represent mean \pm SEM. Abbreviations: WT, wild-type; MN, motor neuron; n.s., not significant.

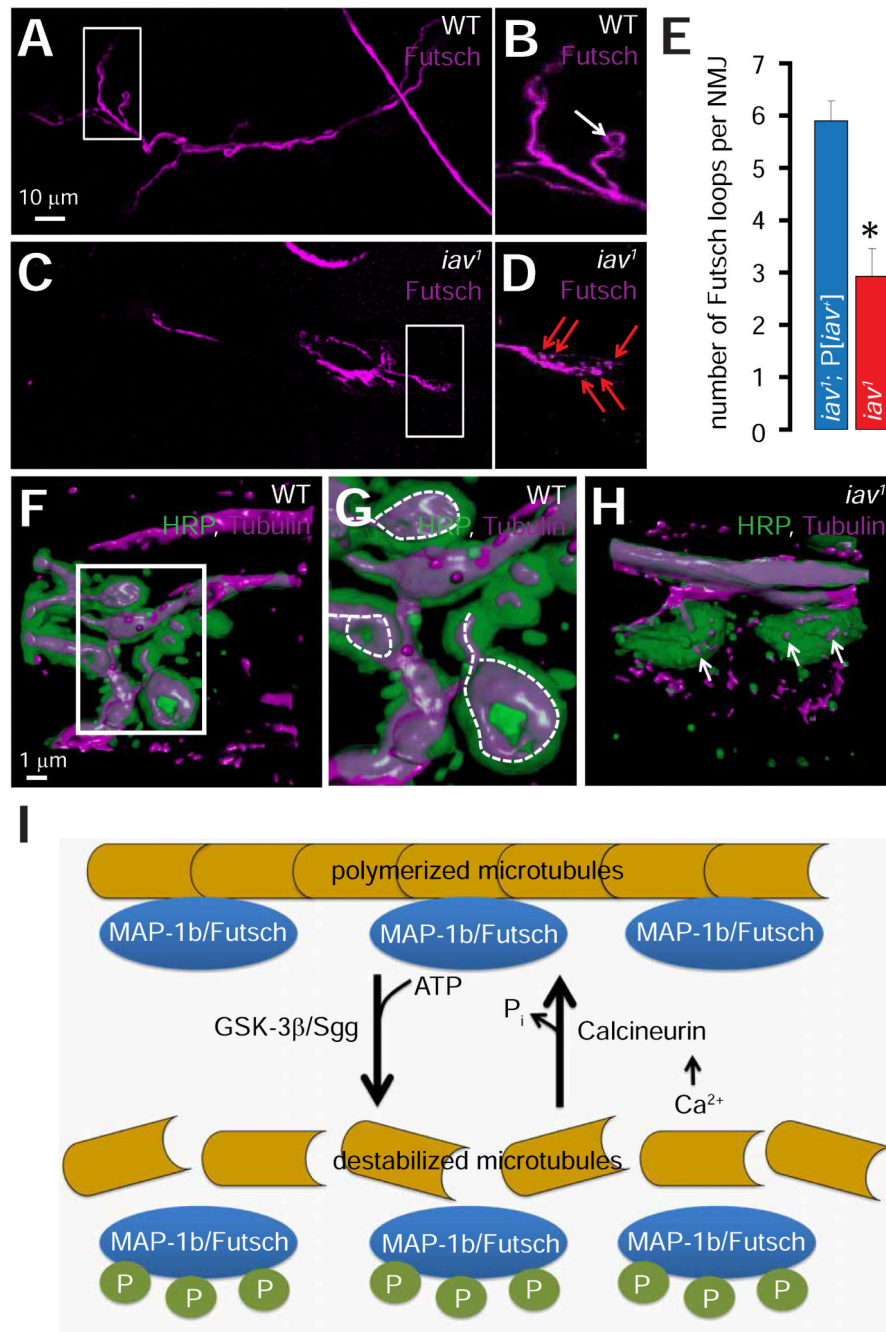


Figure 3. Disruption of the presynaptic microtubule cytoskeleton in *iav¹*

(A) Confocal image of an NMJ from wild-type (WT) larvae stained with antibodies against Futsch (magenta).

(B) Magnification of the boxed region in (A). White *arrow* points to a synaptic Futsch loop.

(C) Same as (A) but in *iav¹* larvae. Scale bar shown in (A) also applies to (C).

(D) Same as (B) but in *iav¹* larvae. Red *arrows* point to synaptic Futsch punctae.

(E) Quantification of the number of Futsch loops per NMJ in the indicated genotypes. *, $p = 3.6 \times 10^{-4}$, Student's t-test, $n = 10-14$ NMJs per genotype.

(F) 3-D reconstruction of a wild-type (WT) synaptic bouton stained with antibodies against HRP (green) and tubulin (magenta).

(G) Magnification of the boxed region in (F). *Dashed-lines* represent synaptic microtubule loops.

(H) Same as (F) but in *iav¹* larvae. *Arrows* point to fragmented microtubules. Scale bar shown in (F) also applies to (H).

(I) Schematic depicting the role of Futsch phosphorylation status on the regulation of presynaptic microtubule stability.

All values represent mean \pm SEM. Abbreviations: MAP-1b, microtubule associated protein-1b; P, phosphorylation.

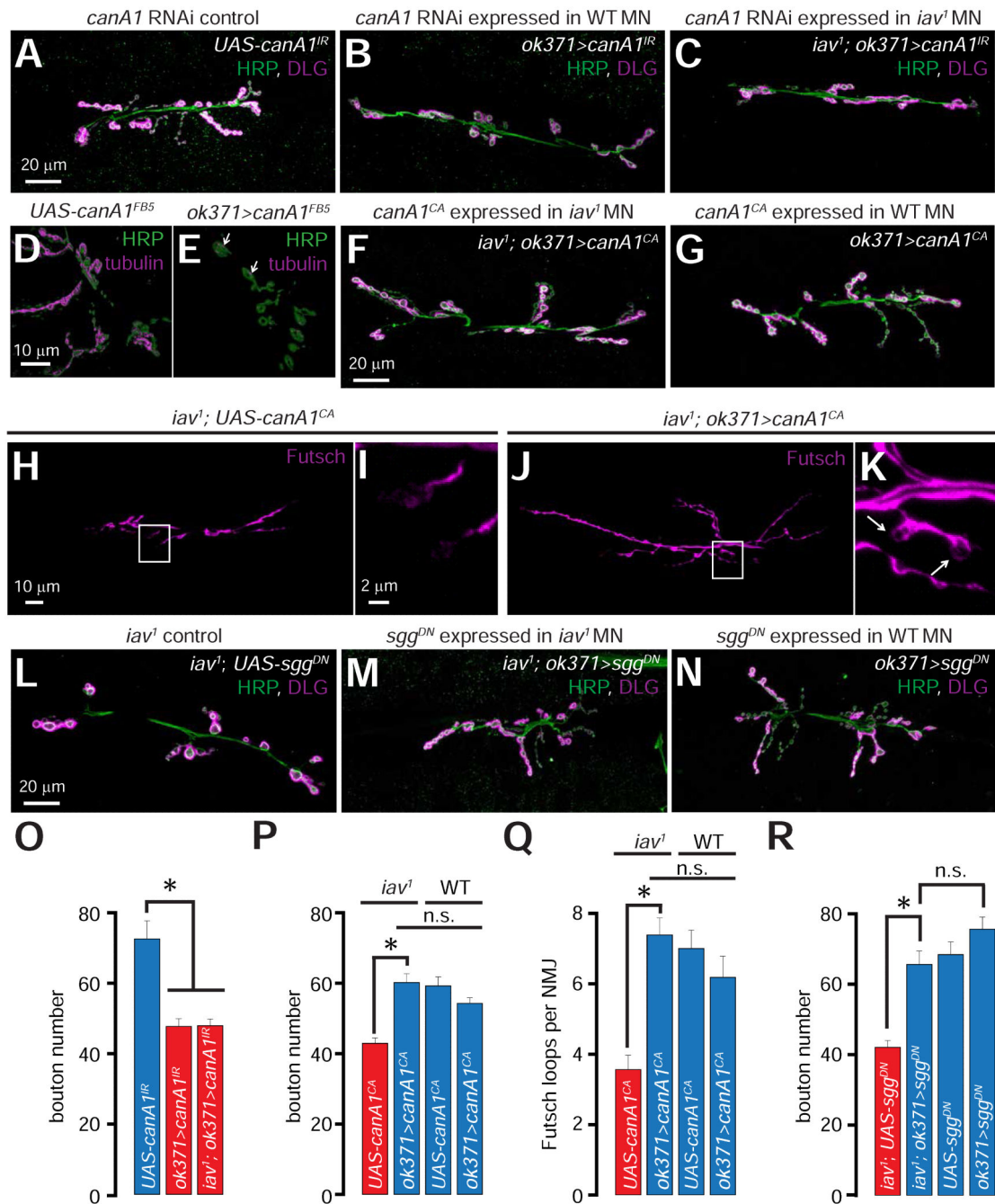


Figure 4. Role of calcineurin in the *iav¹* synaptic growth phenotype

(A-C) Confocal images of NMJs from larvae of the indicated genotypes stained with antibodies against HRP (green) and DLG (magenta). Scale bar shown in (A) also applies to (B-C).

(D-E) 3-D reconstruction of synaptic boutons from larvae of the indicated genotypes stained with antibodies against HRP (green) and tubulin (magenta). Please note that only the microtubules within the NMJ boutons are shown by applying an “HRP mask” (see *Experimental Procedures*). Scale bar shown in (D) also applies to (E).

(F-G) Confocal images of NMJs from larvae of the indicated genotypes stained with antibodies against HRP (green) and DLG (magenta). Scale bar shown in (F) also applies to (G).

(H and J) Confocal images of NMJs from larvae of the indicated genotypes stained with antibodies against Futsch (magenta). Scale bar shown in (H) also applies to (J).

(I and K) Magnification of the boxed regions in (H) and (J) respectively. Scale bar shown in (I) also applies to (K). *Arrows* in (K) point to Futsch loops.

(L-N) Confocal images of NMJs from larvae of the indicated genotypes stained with antibodies against HRP (green) and DLG (magenta). Scale bar shown in (L) also applies to (M-N).

(O) Quantification of the NMJ bouton number in larvae of the indicated genotypes. *, $p = 4.2 \times 10^{-6}$, one-way ANOVA, $n = 12-16$ NMJs per genotype.

(P) Quantification of the NMJ bouton number in larvae of the indicated genotypes. Horizontal bars above the graph indicate data from WT and *iav¹*. *, $p = 2.9 \times 10^{-6}$, unpaired Student's t-test, n.s. represents $p > 0.05$, $n = 16-18$ NMJs per genotype

(Q) Quantification of the number of Futsch loops per NMJ in larvae of the indicated genotypes. Horizontal bars above the graph indicate data from WT and *iav¹*. *, $p = 1.8 \times 10^{-6}$, Student's t-test, n.s. represents $p > 0.05$, $n = 13-16$ NMJs per genotype.

(R) Quantification of the NMJ bouton number in larvae of the indicated genotypes. *, $p = 1.4 \times 10^{-6}$, Student's t-test, n.s. represents $p > 0.05$, $n = 10-18$ NMJs per genotype.

All values represent mean \pm SEM. Abbreviations: MN, motor neuron; WT, wild-type; n.s., not significant.

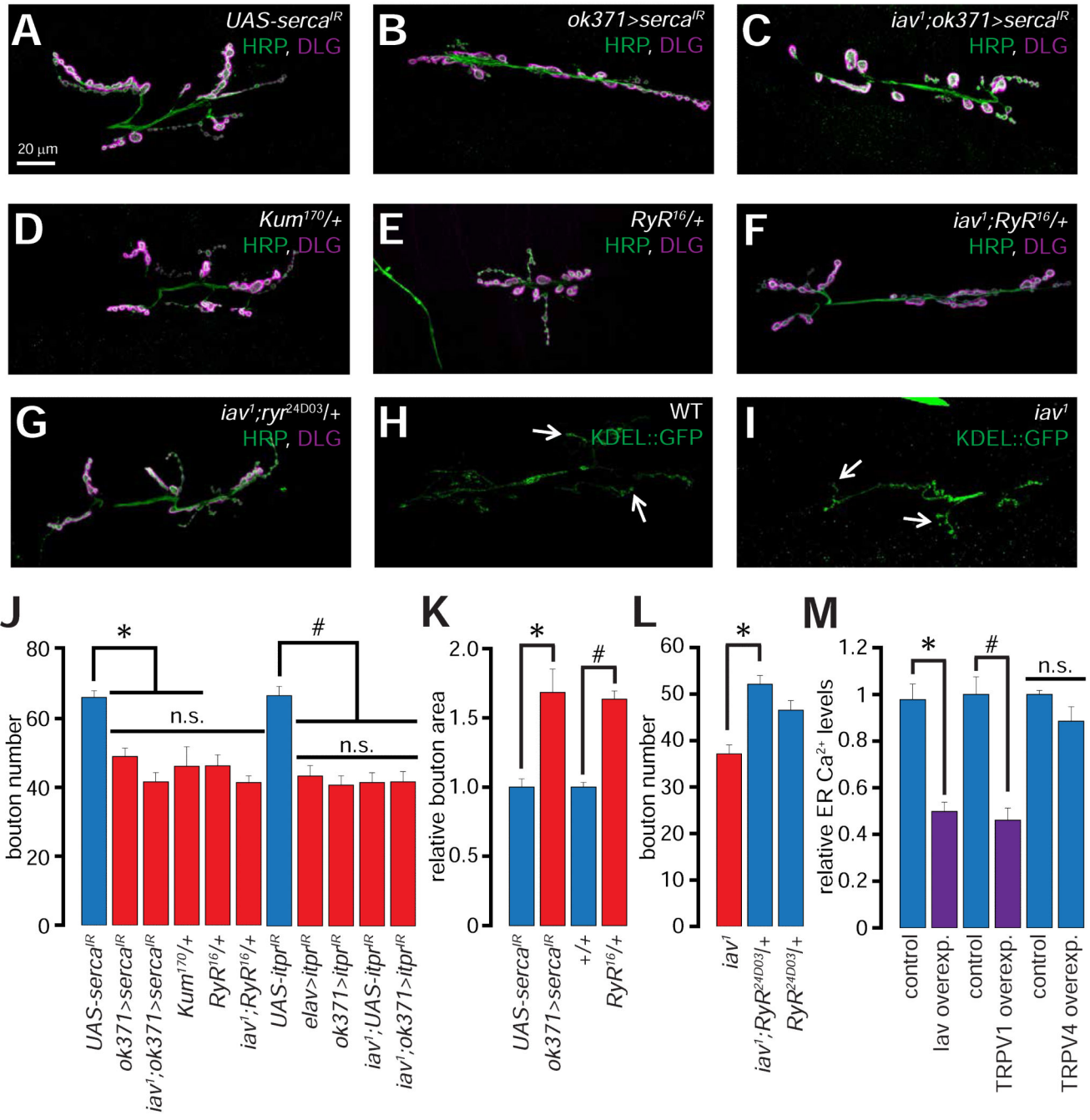


Figure 5. Role of ER Ca²⁺ release in NMJ synapse development

(A-G) Confocal images of NMJs from larvae of the indicated genotypes stained with antibodies against HRP (green) and DLG (magenta).

(H-I) Confocal images of NMJs from larvae of the indicated genotypes expressing Lysozyme-KDEL::GFP (KDEL-GFP) stained with antibodies against GFP (green). *Arrows* point to distal boutons.

Scale bar shown in (A) also applies to (B-G).

(J) Quantification of the NMJ bouton numbers in larvae of the indicated genotypes. *, $p = 5.5 \times 10^{-9}$, one-way ANOVA (comparing the indicated data sets), $n = 9-27$ NMJs per genotype; #, $p = 1.3 \times 10^{-8}$, one-way ANOVA (comparing the indicated data sets), $n = 13-14$ NMJs per genotype.

(K) Quantification of the relative bouton area in larvae of the indicated genotypes. *, $p = 6.4 \times 10^{-4}$, unpaired Student's t-test, $n = 9-11$ NMJs per genotype. #, $p = 6.2 \times 10^{-10}$, unpaired Student's t-test, $n = 14-16$ NMJs per genotype.

(L) Quantification of the NMJ bouton numbers in larvae of the indicated genotypes. *, $p = 3 \times 10^{-6}$, unpaired Student's t-test, $n = 17-21$ NMJs per genotype.

(M) Quantification of the relative ER Ca^{2+} levels as assessed by fura-2 imaging in control N2A cells and in N2A cells overexpressing (overexp.) the indicated TRPV channel. *, $p = 3.4 \times 10^{-10}$, unpaired Student's t-test, $n = 8-9$ independent coverslips containing control or *iav* transfected cells (number of cells per field 8). #, $p = 4 \times 10^{-5}$, unpaired Student's t-test, $n = 8$ independent coverslips containing control or *TRPVI* transfected cells (number of cells per field 10).

All values represent mean \pm SEM. Abbreviations: WT, wild-type; n.s., not significant.

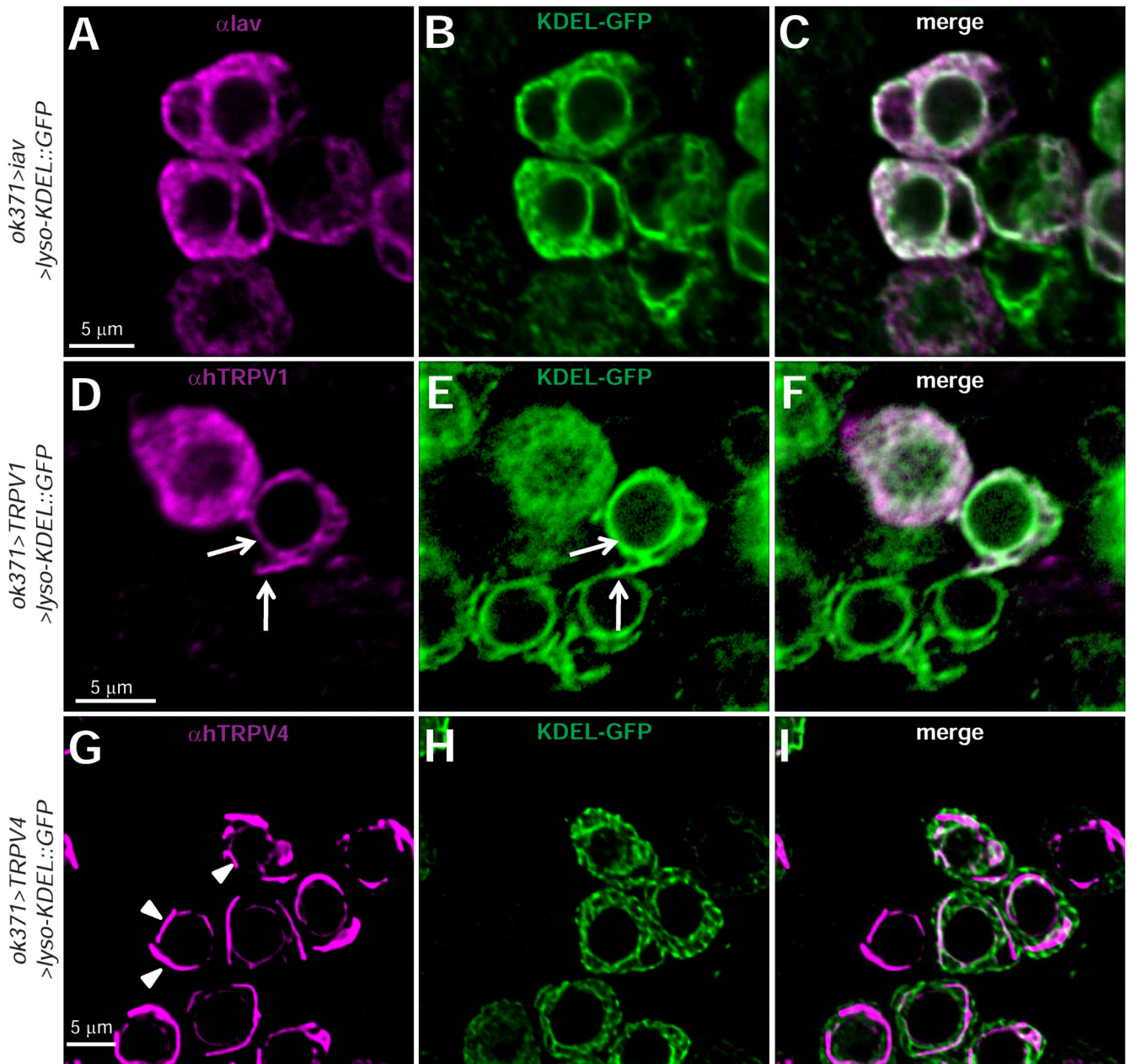


Figure 6. Subcellular distribution of *Iav*, *hTRPV1*, and *hTRPV4* in *Drosophila* larval motor neurons

(A-C) Confocal images of MN cell bodies in ventral nerve cord dissected from larvae expressing *Iav* and KDEL-GFP in motor neurons stained with αIAV (A, magenta), αGFP (B, green), and merge (C). Scale bar shown in (A) also applies to (B-C).

(D-F) Same as (A-C) but with larvae overexpressing *hTRPV1* instead of *Iav*. An antibody against *hTRPV1* was used. Scale bar shown in (D) also applies to (E-F). *Arrows* indicate colocalization between *hTRPV1* and KDEL-GFP in the nuclear envelope and other regions of the ER.

(G-I) Same as (A-C) but with larvae overexpressing hTRPV4 instead of *Iav*. An antibody against hTRPV4 was used. Scale bar shown in (G) also applies to (H-I). The *arrowheads* point to “tubular” structures that are decorated by hTRPV4 in motor neuron cell bodies.

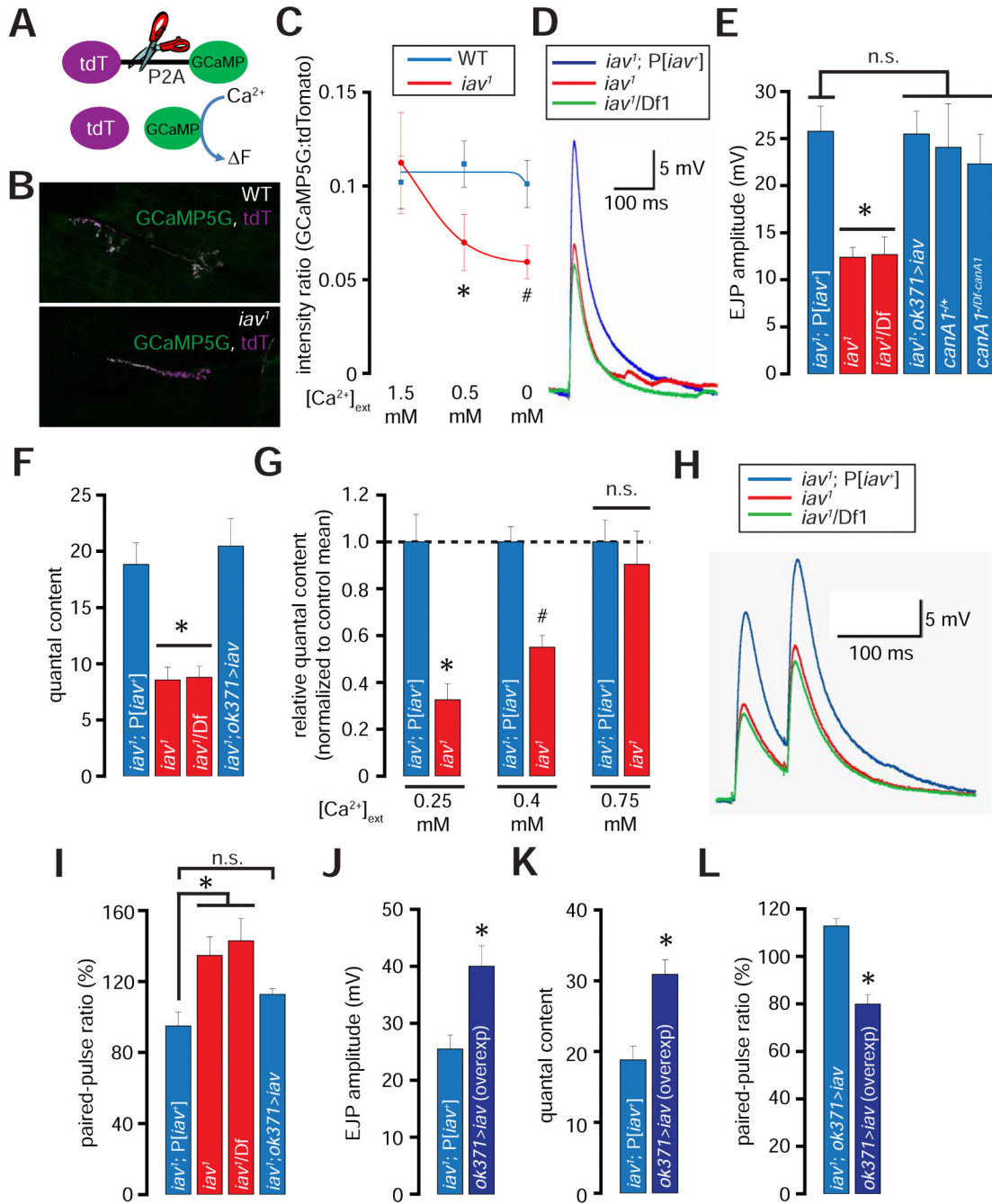


Figure 7. Diminished presynaptic resting Ca^{2+} levels and neurotransmission at the *iav¹* synapses
 (A) Structure of tdTomato-P2A-GCaMP5 (tdT-P2A-GCaMP). Cleavage at the P2A site (indicated by *scissors*) disengages the two fluorophores.
 (B) Confocal images showing the expression of GCaMP5 and tdTomato (tdT) at the NMJ in larvae of the indicated genotypes.
 (C) Quantification of the GCaMP5:tdTomato intensity ratios in wild-type (blue line) and *iav¹* (red line) at the indicated $[Ca^{2+}]_{ext}$. The blue and red curves were obtained by fitting the respective mean values to sigmoidal functions using Origin6 (OriginLab corporation). *, $p =$

0.04, unpaired Student's t-test, n = 7-8 NMJs per genotype; #, p = 0.02, unpaired Student's t-test, n = 7-8 NMJs per genotype.

(D) EJP traces obtained from recordings performed on larval NMJs of the indicated genotypes ($[Ca^{2+}]_{ext}=0.5$ mM).

(E) Quantification of the amplitude of the EJPs obtained from recordings performed on larvae of the indicated genotypes. *, p = 5.1×10^{-4} , one-way ANOVA (comparing all the data sets shown), n = 6-8 NMJs per genotype.

(F) Quantification of the quantal contents obtained from recordings performed on larvae of the indicated genotypes. *, p = 1.1×10^{-5} , one-way ANOVA (comparing all the data sets shown), n = 6-8 animals per genotype.

(G) Quantification of the relative quantal contents in *iav¹* normalized to the *iav¹*; P[*iav⁺*] means at the indicated $[Ca^{2+}]_{ext}$. *, p = 3.5×10^{-4} , unpaired Student's t-test, n = 5-7 NMJs per genotype; #, p = 5.3×10^{-5} , unpaired Student's t-test, n = 7-10 NMJs per genotype.

(H) EJP trace obtained from paired-pulse recordings performed on larval NMJs of the indicated genotypes ($[Ca^{2+}]_{ext}=0.5$ mM).

(I) Quantification of the paired-pulse ratio (% change in the amplitude of the second EJP to that of the first EJP when the two were separated by duration of 50 ms) in the larvae of the indicated genotypes. *, p = 0.01, one-way ANOVA, n = 5-7 animals per genotype.

(J) Quantification of the EJP amplitudes in larvae of the indicated genotypes. *, p = 0.01, Student's t-test, n = 6 NMJs per genotype.

(K) Quantification of the quantal content in larvae of the indicated genotypes. *, p = 0.002, unpaired Student's t-test, n = 6 NMJs per genotype.

(L) Quantification of the paired-pulse ratio in larvae of the indicated genotypes. *, p = 1.5×10^{-4} , unpaired Student's t-test, n = 5-6 NMJs per genotype.

All values represent mean \pm SEM. Abbreviations: WT, wild-type; n.s., not significant.